Journal Name

ARTICLE TYPE

Structure of the Ru, Ag and Te L X-ray emission spectra

T. Rodríguez, A. Sepúlveda, A. Carreras, G. Castellano and J. Trincavelli*

The emission of X-rays in atomic transitions from L-shell vacancy states of Ru, Ag and Te induced by electron incidence was studied. To this end, L X-ray spectra were measured with a wavelength dispersive spectrometer, and processed by a parameter optimization method previously developed. A large set of atomic parameters corresponding to diagram transitions, such as relative transition probabilities, characteristic energies and natural linewidths of the three elements were determined. The results obtained are compared to the data found in the literature, when available. In general terms a good agreement was observed, supporting recent calculations based on the framework of the relativistic many-body problem in atoms. Spectral structures related to satellite and radiative Auger emissions were also analyzed, and energy shifts and relative intensities were determined. Many of these parameters were determined for the first time, which was possible due to the robustness of the spectral processing method used, even in the cases of peak overlapping and weak transitions.

1 Introduction

The analytical prediction of spectra in X-ray spectroscopic techniques requires a good knowledge of several fundamental parameters, like characteristic energies, relative transition probabilities (RTP), fluorescence yields, natural linewidths (Γ), etc. [1,2] Thus, an adequate set of experimental data for these parameters as well as a good description of satellite lines and radiative Auger emission (RAE) structures becomes crucial for a profitable application of techniques such as electron probe microanalysis (EPMA), X-ray fluorescence (XRF) or particle-induced X-ray emission (PIXE). [3,4] On the other hand, the X-rays emitted in atomic transitions contain useful information about atomic structure, and several molecular and solid-state effects. A detailed study of the X-ray emission involving decays from inner-shell hole atomic states is therefore essential for a better understanding of the different processes that can take place as relaxation mechanisms.

Even when the spectral acquisition from pure known standards irradiated with an electron beam may be considered as a routine task, a more difficult challenge is to obtain from these spectra reliable information about the fundamental parameters related to the basic processes involved. To this purpose, a reliable method to process experimental EPMA spectra has been previously developed [5], which takes into account all the physical and instrumental parameters involved: characteristic peaks, bremsstrahlung continuum, multiple ionization bands or peaks, radiative Auger emission (RAE) structures, detection artifacts, etc. The study of X-ray emission in atomic transitions is not only very useful in several spectroscopic techniques but it is also of interest in the field of atomic physics, particularly to test theoretical models and some approximations assumed in them. In the case of L lines, any contribution is especially important due to the scarce data published.

The data available for the elements studied here include experimental determinations re-evaluated by Bearden [6] and Cauchois and Sénémaud [7] for characteristic energies of Ru, Ag and Te, by Ohno et al. [8] for natural linewidths of Ru and Ag, and by Parratt [9] for RTPs, characteristic energies and natural linewidths of Ag. On the other hand, theoretical calculations of characteristic energies for all the transitions involved were carried out by Indelicato et al. [10] and by Deslattes et al. [11], whereas RTPs were assessed by Scofield [12]. These parameters were also predicted by Perkins et al. [13] for all diagram transitions. Finally, a set of natural linewidths compiled by Campbell and Papp [14] is also available for

Facultad de Matemática, Astronomía y Física, Universidad Nacional de Córdoba - Instituto de Física Enrique Gaviola. Ciudad Universitaria, 5000, Córdoba, República Argentina; E-mail: trincavelli@famaf.unc.edu.ar

a large number of transitions for elements from Na to U. Nevertheless, values for several parameters studied were not found in the literature for the elements considered.

In this work, the structure of L X-ray emission spectra induced by electron incidence is studied for Ru, Ag and Te. These spectra were measured by wavelength dispersive spectroscopy and processed using a robust fitting procedure based on a parameter refinement method[5], which takes into account all the spectral features mentioned above. The set of data for Ag published in the pioneering work of Parratt[9] was used to compare the results of satellite relative intensities obtained here. In view of the agreement found, the same parameters were investigated for Ru and Te, elements for which no experimental data for satellite intensities are available. In addition, RAE structures were characterized reporting, for the first time, numerical values for their energy shifts and relative intensities. Some N_{2-5} and O_1 level widths were also determined, for which no experimental data can be found in the literature. Complementarily, relative transition probabilities, characteristic energies and natural linewidths were determined for a number of atomic transitions to the L subshells.

2 Experimental

The spectra were measured with a commercial INCA Wave 700 wavelength dispersive spectrometer (WDS) attached to a Leo 1450VP scanning electron microscope. The Rowland circle has a 21 cm radius, r, in a Johansson type arrangement, i.e., the crystal is bent to radius $2r$ and ground to radius r. This geometry ensures that all X rays originating from the irradiated point at the sample are diffracted along a large region of the crystal surface and are brought to focus at the same point on the detector, thus maximizing the collection efficiency of the spectrometer.

The X-rays diffracted by a PET analyzing crystal were collected by two proportional counters operated in tandem: the first one is a P10 (90%Ar-10%CH$_4$) flow counter and the second one is a sealed Xe counter. All the spectra were collected at 29° take-off angle, by irradiating pure bulk polished standards with a 20 keV electron beam. All three standards were carbon coated to prevent from charge accumulation and thermal damage, particularly in the case of Te, which bears a lower electrical conductivity. The beam currents and live acquisition times for the three spectra were in the ranges of 120–170 nA, and 110–160 minutes, respectively.

With the aim of avoiding thermal fluctuations, the laboratory temperature is kept almost constant; in this way, the spectrometer energy calibration is carried out routinely and the associated uncertainties are negligible. This calibration consists only in adjusting the global shift of the goniometer (*zero* parameter), with the aid of a well known characteristic line from a pure standard.

3 Spectral Analysis

The spectral processing was performed using the software POEMA[5], which is based on a method of atomic and experimental parameter optimization. This method involves the fitting of a function which provides an estimate $\bar{I}_i$ for the measured intensity I_i, as a function of the energy E_i of channel i[15].

$$\bar{I}_i = B(E_i) + \sum_q P_q S_q(E_i) , \qquad (1)$$

where B is the background radiation, S_q is a function accounting for the peak profile, which is Voigt for the characteristic lines, and Gaussian for spectator hole transitions and RAE bands, and P_q is the intensity for the characteristic line q, which is described by

$$P_q = \beta \sigma_\ell^x p_q (ZAF)_q \varepsilon(E_q) , \qquad (2)$$

where β is a constant proportional to the number of incident electrons, $\sigma_\ell^x = \tilde{Q}_\ell \omega_\ell$ is the X-ray production cross section for the ℓ subshell (*i.e.*, the product of the final vacancy production cross section $\tilde{Q}_\ell$ and the fluorescence yield ω_ℓ); p_q and E_q are the relative transition probability and the characteristic energy of the line q, respectively; Z, A and F are the correction factors for atomic number, absorption and fluorescence, respectively[16], and ε is the spectrometer efficiency. The corresponding efficiency curve was obtained from the comparison of two measurements of a particular spectrum: one of them carried out with an energy dispersive spectrometer and the other one with the WDS whose efficiency is searched. More details about the method for efficiency determination, and the obtained curve can be found elsewhere[17].

In the case of transitions to L shells, the final vacancy production cross sections are related to the ionization cross sections Q_ℓ by

$$\tilde{Q}_{L_1} = Q_{L_1} \qquad (3)$$

$$\tilde{Q}_{L_2} = Q_{L_2} + f_{12}\tilde{Q}_{L_1} \qquad (4)$$

$$\tilde{Q}_{L_3} = Q_{L_3} + f_{13}\tilde{Q}_{L_1} + f_{23}\tilde{Q}_{L_2} , \qquad (5)$$

where f_{kj} is the probability of a Coster-Kronig transition from an initial state with a vacancy in the L_k subshell to a final state with a vacancy in the L_j subshell.

The optimization method consists in minimizing the quadratic differences between the experimental spectrum and the analytical function proposed (1):

$$\chi^2 = \frac{1}{N_c - N_p} \sum_{i=1}^{N_c} \frac{(\bar{I}_i - I_i)^2}{I_i} , \qquad (6)$$

where N_c is the number of channels and N_p is the number of parameters to be refined.

The global parameters refined by POEMA are: the scale factor

involved in the bremsstrahlung prediction, the peak scale factor β, the spectrometer calibration parameters and the description of instrumental peak broadening. Individual parameters associated to each peak or to specific peak groups can be also optimized by the program, such as characteristic energies, relative transition probabilities, natural linewidths, etc. Each of the latter represents the Lorentzian component of the Voigt profile, whereas the instrumental broadening coefficient is related to the Gaussian component. The refinement procedure must be carried out through a cautious sequence of minimization steps in order to get the best fit of the experimental spectrum. In addition, the physical validity of the results obtained in each step must be evaluated to avoid local minima in the function to be minimized.

Roughly, the strategy for the spectral fitting was to sequentially refine the global parameters in a wide spectral region including all the characteristic peaks in a first stage. Then the individual parameters characteristic energies, RTPs and natural linewidths where optimized separately, which allowed us to proceed with the refinement of the parameters related to satellite lines and RAE structures. Finally, all the parameters where optimized together.

The uncertainties related to the parameters obtained were estimated by propagating the errors of the experimental channel intensities by numerical differentiation[18]. The meaning of this procedure is to account for the influence of the statistical errors inherent to the counts registered at each spectrometer position on the estimated uncertainty for each optimized parameter. In order to perform these calculations, all the relevant models involved in the analytical description of the spectrum ($\bar{I}_i$) were assumed to be exact; this approximation is reasonable, since the main contributions to the resulting uncertainties are due to experimental statistical errors, which are more determinant in the case of weak lines.

4 Results and discussion

Fig. 1 shows the experimental spectra of Ru, Ag, and Te. As can be seen, a good fit was achieved, with $\chi^2 < 2$ in all the cases. In the case of Ru, Mo traces are evidenced through two weak L lines. These lines were properly taken into account during the spectrum fitting procedure, so they did not affect the determination of Ru atomic parameters.

All the peaks observed in the spectra were identified as diagram lines (labeled in the figures), spectator hole transitions or RAE structures. For the sake of clarity, only spectator hole transitions will be referred to as satellite lines. The shoulders appearing close to some of the diagram lines are satellite and RAE structures, which are discussed in subsection 4.4.

4.1 Characteristic energies

With the purpose of validating the calibration and the optimization procedure performed, the characteristic energies obtained in this work are compared with results published by Bearden[6], Cauchois and Sénémaud[7] and Deslattes et al.[11] in Table 1. Data published by Perkins et al.[13] strongly deviate from these sets of data, and were thus excluded from the present comparison. The software POEMA allows for the optimization of the calibration parameters *zero* and *gain*, which relate the analyzer crystal position to the corresponding wavelength[15]. For the present assessments, the *gain* value was taken from the default calibration settings, while the *zero* value was fitted so that the energy of the most intense peak in each spectrum (L_3M_5) matches the value reported by Bearden[6], in each case. Thus, the possible influence of the goniometer offset is avoided. To estimate the uncertainty of each transition energy, the fitting error was added in quadrature with the error reported by Bearden[6] for the line L_3M_5 taken as reference.

In Fig. 2, a comparison between the characteristic energies obtained in this work and data available in the literature is given. The differences between the data given by the other authors and the ones determined in this work are below 1.5 eV in 80% of the cases. The remaining cases correspond to four transitions of Ru, three of Ag and five of Te. In the case of Ru, the characteristic lines $L_3N_{4,5}$, L_2N_1 and L_2N_4 reported by Deslattes et al.[11] show some discrepancy with the data obtained here, which are slightly lower; the other two data sets, however, agree well with the present results. In addition, the Ru L_1N_2 and L_1N_3 transitions are considered as a doublet in Bearden[6] and Cauchois and Sénémaud[7]; in situations like this, the comparisons displayed in Table 1 were carried out with the average of the values reported here for the transitions involved. In this pair, although certain discrepancy with Bearden[6] and Cauchois and Sénémaud[7] can be seen, a reasonable agreement with Deslattes et al.[11] is observed.

For Ag, the energy of the L_1N_2–L_1N_3 pair obtained in this work is below the values reported by the other three authors; nevertheless, although the disagreement between the present value and the data given in Bearden[6] and Deslattes et al.[11] is considerable, the discrepancy between these authors and Cauchois and Sénémaud[7] is even greater. In addition, the energies reported in Deslattes et al.[11] for the transitions L_3N_1 and L_2N_1 are higher than the obtained in this work and in the other two references.

Finally, for Te, the greater discrepancies correspond to the L_3N_1, L_2N_1, $L_1O_{2,3}$ and L_3O_1 transitions, which represent very weak lines (less than 1% of the total intensity of the corresponding group in each case), and also to the L_1N_2–L_1N_3 pair, which is considered a doublet for Bearden[6] and Cauchois and Sénémaud[7]. It must be noticed, however, that for the last case, the differences between the results presented here and some of the data compared are similar to the discrepancies arising among the other data themselves. This doublet is not properly described with only two peaks not only for Te but also for Ag. It is important mentioning that according to Deslattes et al.[11], there is a dipolar
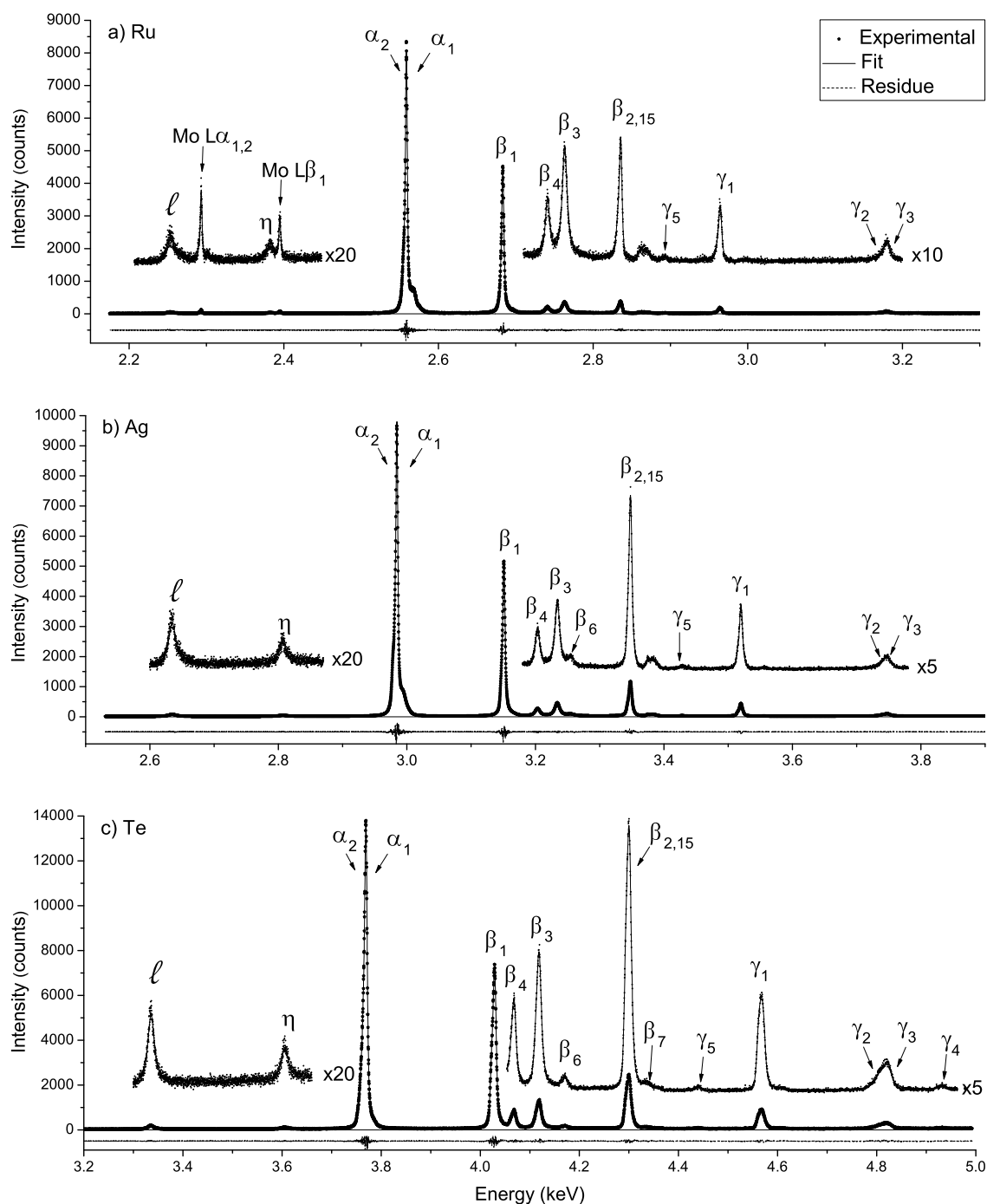
Fig. 1 L-spectra measured at 20 keV: a) Ru, b) Ag, c) Te. The insets show magnified views of the regions with weak peaks.

Table 1 Characteristic energies (in keV). Numbers in parentheses indicate the estimated uncertainties in the last digit.
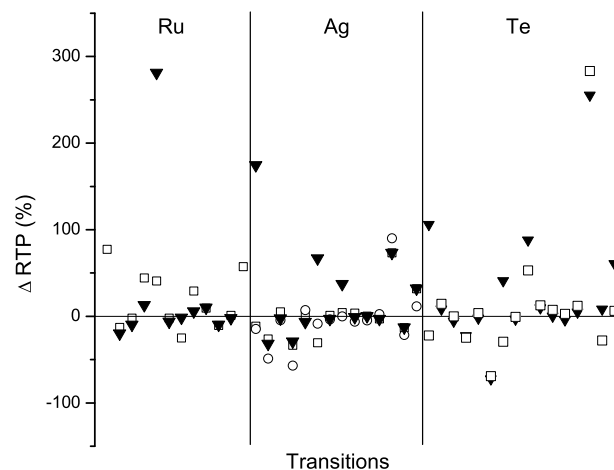
Trans.	Ru				Ag				Te			
	This work	Ref.[6]	Ref.[7]	Ref.[11]	This work	Ref.[6]	Ref.[7]	Ref.[11]	This work	Ref.[6]	Ref.[7]	Ref.[11]
$L_3M_1(l)$	2.2541(1)	2.25280	2.25270	2.254	2.6348(1)	2.63370	2.63363	2.634	3.3357(1)	3.33558	3.33545	3.335
$L_3M_4(\alpha_2)$	2.5543(3)	2.55431	2.55438	2.5542	2.9786(2)	2.97821	2.97824	2.979	3.7591(3)	3.75879	3.75870	3.760
$L_3N_1(\beta_6)$					3.2550(3)	3.25603	3.25584	3.258	4.1698(3)	4.17325	4.17314	4.174
$L_3N_{4,5}(\beta_{2,15})$	2.8358(2)	2.83600	2.83598	2.8383	3.34801(4)	3.34781	3.34783	3.3478	4.3011(1)	4.30170	4.30160	4.3017
$L_3O_1(\beta_7)$									4.3373(5)	4.32980	4.32999	
$L_2M_1(\eta)$	2.3819(2)	2.38197	2.38190	2.383	2.8069(2)	2.80610	2.80607	2.807	3.6057(2)	3.60590	3.60578	3.605
$L_2M_4(\beta_1)$	2.68324(3)	2.68323	2.68326	2.683	3.15101(2)	3.15094	3.15109	3.151	4.02919(7)	4.02963	4.02953	4.030
$L_2N_1(\gamma_5)$	2.8918(4)	2.89180	2.89179	2.896	3.4282(5)	3.42832	3.42819	3.430	4.4402(6)	4.44370	4.44359	4.445
$L_2N_4(\gamma_1)$	2.9645(2)	2.96450	2.96447	2.9666	3.51996(5)		3.51962	3.5193	4.5711(1)	4.57093	4.57084	4.571
$L_1M_2(\beta_4)$	2.74110(7)		2.74110	2.741	3.20343(7)	3.20346	3.20332	3.203	4.0684(1)	4.06952	4.06944	4.069
$L_1M_3(\beta_3)$	2.76326(6)	2.76340	2.76327	2.763	3.23416(5)	3.23446	3.23427	3.234	4.11917(9)	4.12048	4.12040	4.120
$L_1M_4(\beta_{10})$									4.3551(9)	4.35516	4.35499	4.356
$L_1M_5(\beta_9)$					3.4381(6)	3.43917	3.43901	3.438	4.3671(9)	4.36716	4.36698	4.366
$L_1N_2(\gamma_2)$	3.176(8)	3.18090	3.18109	3.176	3.7410(6)	3.74320	3.74965	3.746	4.807(1)	4.82910	4.82905	4.821
$L_1N_3(\gamma_3)$	3.181(2)			3.183	3.7484(3)	3.74980		3.748	4.8222(6)			4.823
$L_1O_{2,3}(\gamma_4)$									4.9327(7)	4.93690	4.93696	
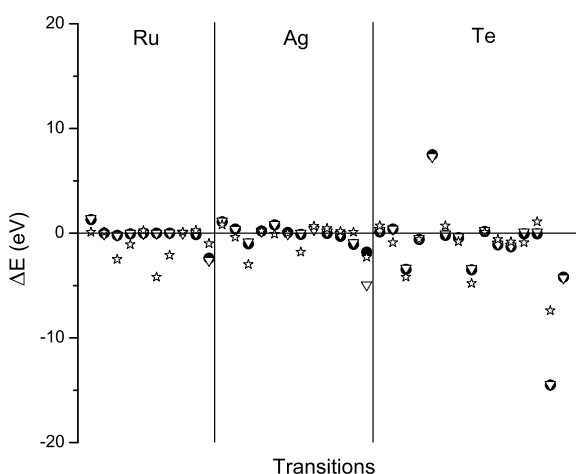
Fig. 2 Differences of the characteristic energies obtained in this work respect to the values reported by other authors. Solid circles: Ref.[6], open triangles: Ref.[7], open stars: Ref.[11]. The transitions are ordered as in Table 1.

Fig. 3 Percent differences of the RTP data obtained here relative to the values reported by other authors. Open circles: Ref.[9], solid triangles: Ref.[13], open squares: Ref.[19]. The transitions are ordered as in Table 2.

forbidden transition (L_1N_1) with energy close to the L_1N_2–L_1N_3 peak. Unfortunately, there is no information about the RTP of this decay, which hampers its inclusion in the spectral fit.

It must be noted that the characteristic energies of Ru L_1M_2 and Ag L_2N_4 lines were not reported by Bearden[6]. These energies, however, were measured by Cauchois and Sénémaud[7] and assessed by Deslattes et al.[11], and they are in very good agreement with the present data.

The very good agreement between the present values and previous experimental data[6] in most of the transitions studied suggests that the uncertainties due to the calibration procedure (and not taken into account by the propagation of errors explained above) are negligible. Any error in the instrument calibration would translate into systematic deviations along all the energy range considered, reducing the accuracy of the results obtained, which clearly is not the case.

4.2 Relative transition probabilities

The RTP of an L_kX_j line is the probability of the corresponding transition relative to all the decays to the L_k subshell. The RTP values obtained in this work are presented in Table 2, along with the data reported by Scofield[19], Perkins et al.[13] and Parratt[9]. To normalize the RTPs, all the transitions observed experimentally were taken into account. For Te, the set of transitions coincides with the one reported by Scofield[19]. In the case of Ag, the weak L_1M_4 line was not appreciated in the spectrum. This transition amounts only 0.3% of all the decays to the L_1 subshell, according to the data available in the literature[13,19]. In addition, the intensity of the Ru L_3N_1 line could not be determined, because this line is too low, and located between the much more intense L_1M_2 and L_1M_3 lines. However, this line represents around 0.6% of the L_1 group according to previous theoretical predictions[19].

Figure 3 displays a comparison between the RTPs obtained in this work and data published by the other authors. The present results show a good agreement in the case of the most intense

Table 2 Relative transition probabilities. Numbers in parentheses indicate the estimated uncertainties in the last digit.

Trans.	Ru			Ag				Te		
	This work	Ref. [19]	Ref. [13]	This work	Ref. [9]	Ref. [19]	Ref. [13]	This work	Ref. [19]	Ref. [13]
$L_3M_1(l)$	0.0189(5)	0.0335	0.1158	0.0371(5)	0.0317	0.0329	0.1019	0.0411(4)	0.0320	0.0847
$L_3M_4(\alpha_2)$	0.106(8)	0.0924	0.0849	0.121(6)	0.0620	0.0895	0.0828	0.075(4)	0.0859	0.0812
$L_3M_5(\alpha_1)$	0.833(6)	0.8150	0.7530	0.752(4)	0.7198	0.7910	0.7341	0.763(3)	0.7620	0.7197
$L_3N_1(\beta_6)$				0.0093(4)	0.0040	0.0062	0.0066	0.0089(2)	0.0067	0.0069
$L_3N_{4,5}(\beta_{2,15})$	0.041(2)	0.0592	0.0463	0.0799(5)	0.0857	0.0805	0.0747	0.109(2)	0.1130	0.1068
$L_3O_1(\beta_7)$								0.0029(3)	0.0009	0.0008
$L_2M_1(\eta)$	0.0196(9)	0.0276	0.0747	0.0377(9)	0.0345	0.0262	0.0629	0.0344(8)	0.0243	0.0485
$L_2M_4(\beta_1)$	0.927(5)	0.9076	0.8698	0.877(7)	0.8471	0.8857	0.8509	0.859(5)	0.8544	0.8319
$L_2N_1(\gamma_5)$	0.0068(6)	0.0051	0.0067	0.0048(5)	0.0048	0.0050	0.0066	0.0034(3)	0.0052	0.0064
$L_2N_4(\gamma_1)$	0.0462(9)	0.0597	0.0489	0.0802(9)	0.0752	0.0831	0.0795	0.103(2)	0.1162	0.1132
$L_1M_2(\beta_4)$	0.288(5)	0.3157	0.3174	0.316(4)	0.3016	0.3166	0.3165	0.311(8)	0.3340	0.3113
$L_1M_3(\beta_3)$	0.597(6)	0.5351	0.5391	0.543(5)	0.5568	0.5267	0.5266	0.520(6)	0.5353	0.4987
$L_1M_4(\beta_{10})$								0.0041(6)	0.0046	0.0043
$L_1M_5(\beta_9)$				0.003(4)	0.0057	0.0052	0.0052	0.0018(5)	0.0069	0.0064
$L_1N_2(\gamma_2)$	0.054(6)	0.0546	0.0528	0.065(5)	0.0510	0.0565	0.0566	0.076(3)	0.1125	0.0641
$L_1N_3(\gamma_3)$	0.060(6)	0.0945	0.0906	0.072(5)	0.0804	0.0950	0.0951	0.080(3)		0.1049
$L_1O_{2,3}(\gamma_4)$								0.0064(6)	0.0068	0.0103

lines; particularly with the theoretical data given by Scofield[19]. On the other hand, for some transitions amounting less than 5% of the intensities corresponding to decays to the same subshell, differences are important. The discrepancy of the RTP reported by Perkins et al.[13] for the L_3M_1 line is particularly large for the three elements studied, as well as for the Ru L_2M_1 line. It should be noticed that no experimental data are available for Ru and Te; despite the differences observed, a comparison with the present results clearly favor the data reported by Scofield[19] as compared to Perkins et al. data base.[13] Regarding silver, a good agreement was found respect to the experimental data published by Parratt[9], except for three cases: L_3M_4, L_3N_1 and L_1M_5 lines. The last two lines are very weak transitions (less than 1% of the group), whereas the first one corresponds to the $L\alpha_2$ decay, which is very close to the intense $L\alpha_1$ line. The RTP reported by Parratt for the latter shows also a disagreement respect to the theoretical predictions (see Table 2), which suggests a difficulty in its determination. It must be mentioned that the spectrometer used by Parratt had a better resolution than the one involved in the present work; nevertheless, the spectral processing method used here is quite more reliable.

4.3 Natural linewidths

A diagram line can be well described by a Voigt profile[15] V, which is the convolution of a Lorentzian, representing the emitted profile, and a Gaussian function, associated with the instrumental peak broadening:

$$V(x) = \frac{\sqrt{\ln 2}\, \gamma_L}{\pi^{3/2} \gamma_G} \int_{-\infty}^{\infty} \frac{\exp[-\ln 2 (x'/\gamma_G)^2]}{(x - x')^2 + \gamma_L^2} dx' \tag{7}$$

where γ_L and γ_G are the half width at half maximum for the Lorentzian and Gaussian contribution, respectively. In other words, γ_L is the half of the natural linewidth, and the instrumental broadening can be derived from the Bragg's law as a function of the photon energy E:

$$\gamma_G = \sqrt{2 \ln 2}\, \Delta\theta E \sqrt{\left(\frac{2d}{hc} E\right)^2 - 1} \tag{8}$$

where d is the is the interplanar spacing of the crystal, h is the Planck constant and c is the speed of light in vacuum. Thus, each Voigtian peak at energy E can be described by means of two parameters, refinable with POEMA: γ_L, related to its natural linewidth, and the angular divergence $\Delta\theta$ of the analyzer crystal; the latter being common to all the peaks present in the spectrum.
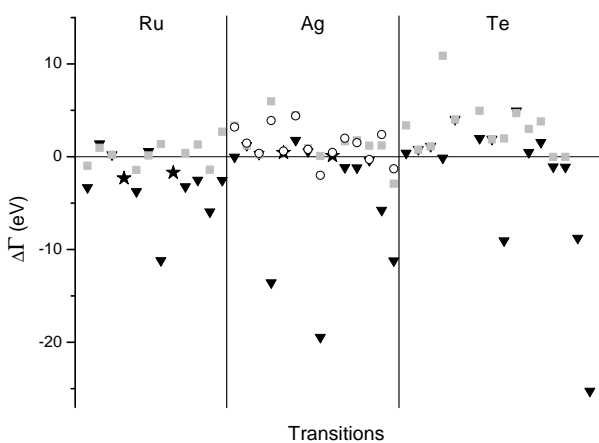
Table 3 shows the natural linewidths obtained in this work along with data calculated by adding the energy level widths involved in each decay published by Perkins et al.[13] and by Campbell and Papp[14]. Natural linewidths reported by Ohno et al.[8] and by Parratt[9] for some transitions are also shown. It is worth mentioning that linewidths obtained here for the L_3O_1 and $L_1O_{2,3}$ decays of Te were not reported up to now in the literature.

Fig. 4 presents a comparison between the natural linewidths obtained here and values reported in the literature, in which a good agreement can be observed, except for the values published by Perkins et al.[13], where differences up to 20 eV were found. The widths corresponding to Te $L_3N_{4,5}$ and L_2N_4 lines determined in this work exceed the double of the values reported by Perkins et al.[13] and by Campbell and Papp[14]. Nevertheless, the agreement between these two sets of data in these cases is expectable because the natural linewidths published by the latter were calculated from the N_4 and N_5 level widths tabulated by the former, and from L level widths, which are known with a higher accuracy and are similar in both databases.

It must be pointed out that there are several energy levels

Table 3 Natural linewidths (in eV). Numbers in parentheses indicate the estimated uncertainties in the last digit.

Trans.	Ru				Ag					Te		
	This work	Ref. [13]	Ref. [14]	Ref. [8]	This work	Ref. [13]	Ref. [14]	Ref. [8]	Ref. [9]	This work	Ref. [13]	Ref. [14]
$L_3M_1(l)$	8.1(3)	11.41	9.07		13.9(3)	13.91	10.55		10.7	16.2(3)	15.79	12.82
$L_3M_4(\alpha_2)$	3.43(9)	2.020	2.46		3.66(5)	2.42	2.45		2.2	3.9(2)	3.1	3.14
$L_3M_5(\alpha_1)$	2.25(2)	2.020	2.04		2.70(2)	2.43	2.46		2.34	4.25(2)	3.11	3.14
$L_3N_1(\beta_6)$					12.5(7)	26.05	6.55		8.6	15.9(7)	16.03	5.02
$L_3N_{4,5}(\beta_{2,15})$	3.0(2)			5.3	4.32(8)			3.9	3.72	6.8(1)	2.76	2.79
$L_3O_1(\beta_7)$										11.2(4)		
$L_2M_1(\eta)$	7.8(5)	11.55	9.23		15.2(6)	13.42	10.72		10.8	18.0(6)	16.01	13.04
$L_2M_4(\beta_1)$	2.74(3)	2.16	2.62		3.18(3)	2.6	2.62		2.4	5.23(4)	3.32	3.36
$L_2N_1(\gamma_5)$	7.3(7)	18.48	5.93		6.8(5)	26.23	6.72		8.8	7.2(2)	16.25	5.24
$L_2N_4(\gamma_1)$	3.8(4)			5.5	4.4(1)			4.3	3.95	7.7(3)	2.76	3.01
$L_1M_2(\beta_4)$	6.5(2)	9.72	6.1		7.9(2)	9.04	6.25		5.9	8.4(4)	7.91	5.4
$L_1M_3(\beta_3)$	7.4(1)	9.9	6.1		8.1(1)	9.28	6.35		6.6	9.9(2)	8.33	6.1
$L_1M_4(\beta_{10})$										2.7(7)	3.78	2.72
$L_1M_5(\beta_9)$					5.3(9)	5.71	4.11		5.6	2.7(7)	3.79	2.72
$L_1N_2(\gamma_2)$	5.7(7)	11.63	7.1		13.4(8)	19.16	12.2		11.0	19.7(8)	28.47	
$L_1N_3(\gamma_3)$	9.4(9)	11.93	6.7		8.9(8)	20.11	11.8		10.2	14.1(6)	39.35	
$L_1O_{2,3}(\gamma_4)$										7.7(4)		

Fig. 4 Differences between the natural linewidths obtained in this work and the values reported by other authors. Solid triangles: Ref. [13], stars: Ref. [8], open circles: Ref. [9], solid squares: Ref. [14]. The transitions are ordered as in Table 3.

Table 4 Atomic level widths (in eV). Numbers in parentheses indicate the estimated uncertainties in the last digit.

	N_2	N_3	N_4	N_5	O_1
Ru	2(1)	6(1)	1.8(5)	1.1(3)	
Ag	10(1)	5(1)	2.1(3)	2.2(2)	
Te	17.5(9)	11.9(7)	4.9(4)	4.2(3)	8.6(5)

4.4 Satellite transitions and Radiative Auger emissions

Tables 5 and 6 show the relative energies and areas of the satellite lines and RAEs, respectively, associated with the main transitions studied. Every relative area displayed was calculated as the ratio of each particular peak area to the sum of the parent line area and the areas of all the RAEs and satellites arising from it. In Table 5, data published by Cauchois and Sénémaud [7] for the three elements considered, and by Parratt [9] for silver, are also presented.

In Figs. 5–7 the Lα (a) and L$\beta_{2,15}$ (b) spectral regions of Ru, Ag and Te are displayed in detail. These figures show the experimental data and the fitting curves. The contributions of diagram lines were modeled with Voigt profiles, whereas satellite bands and RAE structures were described with Gaussian profiles. Gaussian functions proved to be appropriate to fit the spectator hole transition bands, which are typically a set of several transitions of similar energies. On the other hand, even when RAE structures present a tail at the low energy side, Gaussian functions were chosen to describe them because with a few fitting parameters a good description of the structures was achieved. In all the cases, the adopted criterion consists in achieving a good fit with the fewest possible lines. As displayed in Figs. 5–7, one or two satellite lines and one RAE band appear associated with the L$\beta_{2,15}$ line for the three elements. In the case of the Lα doublet, four satellite transitions and one RAE band can be seen for both Ru and Ag, while one satellite and two RAEs are present in the Te spectrum. In the case of Te, the two RAE bands observed were

whose widths are not available in the literature; particularly, O levels, and N_4 and N_5 levels for elements with Z < 50. Table 4 shows some N and O level widths determined from the natural linewidths obtained in this work and from L level widths taken from Campbell and Papp [14]. To estimate each uncertainty, the error of the natural linewidth involved was added in quadrature with the error associated with the L level width. For the natural linewidths, the errors shown in Table 3 were used, while for the L level widths, the error estimation given in the table A of Campbell and Papp [14] was considered, taking the highest value when an error range is suggested.

Table 5 Relative energies and areas of satellite bands.[a] Sum of all the satellites related to the corresponding group. In the case of the data taken from Parratt[9], other lines reported in the original paper and not displayed here were considered.

Diagram line	ΔE (eV)			Relative area (%)	
	This work	Ref.[7]	Ref.[9]	This work	Ref.[9]
Ru $L_3M_5(\alpha_1)$	5.8(6)	6.85		0.53(7)	
	9.3(9)	9.51		11.2(3)	
	16.7(9)	16.51		0.70(5)	
	19.4(8)	20.16		1.66(6)	
$L_3N_{4,5}(\beta_{2,15})$	25(1)	24.13		1.4(4)	
	29.7(3)	29.29		25(2)	
$L_2M_4(\beta_1)$	12.2(4)	13.16		2.3(2)	
Ag $L_3M_5(\alpha_1)$	9.8(3)	10.71	10.66	7.8(1)	4.5
	13.1(6)	13.97	14.18	3.9(2)	2.7
	18.4(2)	18.99	18.73	0.64(7)	1.4
	37.7(3)			0.05(1)	
				12.5[a]	10.5[a]
$L_3N_{4,5}(\beta_{2,15})$	26.6(4)	29.22	26.62	1.3(1)	3.7
	34.2(3)	33.84	32.47	11.5(3)	2.0
				12.9[a]	13.0[a]
$L_2M_4(\beta_1)$	12.5(7)	8.92	8.85	2.20(8)	1.6
		15.39	15.32		1.6
				2.2[a]	4.0[a]
$L_2N_4(\gamma_1)$	35.9(8)	35.70	35.24	2.6(3)	2.2
				2.6[a]	3.6[a]
Te $L_3M_5(\alpha_1)$	15.9(3)	17.03		1.13(4)	
$L_3N_{4,5}(\beta_{2,15})$	5.7(3)	8.03		2.1(2)	

Table 6 Relative energies and areas of RAE structures.

Diagram line	ΔE (eV)	Relative area (%)
Ru $L_3M_5(\alpha_1)$	-2.6(3)	3.9(2)
$L_3N_{4,5}(\beta_{2,15})$	-2.7(8)	25(1)
$L_2M_4(\beta_1)$	-2.4(4)	7.4(9)
$L_2N_4(\gamma_1)$	-2.4(9)	21(3)
Ag $L_3M_5(\alpha_1)$	-3.1(2)	3.7(1)
$L_3N_{4,5}(\beta_{2,15})$	-4.4(6)	5.2(2)
$L_2M_4(\beta_1)$	-3.8(4)	6.8(1)
$L_2N_4(\gamma_1)$	-5.1(7)	5.3(4)
Te $L_3M_4(\alpha_2)$	-4.8(3)	18.3(9)
$L_3M_5(\alpha_1)$	-5.2(1)	13.6(1)
$L_3N_{4,5}(\beta_{2,15})$	-6.0(3)	29(2)
$L_2M_4(\beta_1)$	-5.6(1)	19.5(2)
$L_2N_4(\gamma_1)$	-7.3(4)	45(1)
$L_1M_2(\beta_4)$	-4.9(1)	19.0(9)
$L_1M_3(\beta_3)$	-4.9(1)	16.3(5)

assigned to the $L\alpha_1$ and $L\alpha_2$ lines. This assignment led to similar shifts of the RAEs with respect to the corresponding parent lines, in consistency with what was observed for the other two elements.

As can be seen in Table 5, the satellite lines identified can be properly associated with the ones reported by Cauchois and Sénémaud[7] and by Parratt[9]. These authors also report other satellite lines, particularly for Te, not observed here probably due to their low intensity.

It can be observed that, in the case of silver, even when the relative areas of the satellite lines present certain discrepancies with the data published by Parratt, the sums of the relative areas corresponding to the same parent line agree when all the satellite lines reported by this author are taken into account. It must be noted that the energy of the satellite lines can be considered independent of the excitation source, unlike their relative intensities; particularly, the multiple spectator hole satellites are markedly more intense when irradiating with ions. Nevertheless, the agreement found with the data published by Parratt is expectable because the 15 keV incident electron source involved in Parratt[9] is similar to the one used in this work (20 keV electrons), both energies being well above several combinations of double and triple ionization energies. It is worth mentioning that the relative areas for Ru and Te satellite bands were not reported previously in the literature.

When the relaxation energy of an L_iR_j transition is shared between a photon of energy $h\nu$ and an Auger electron ejected from the T_k shell with kinetic energy E_{el}, the energy balance can be written as:

$$h\nu + E_{el} = E(L_i) - E(R_j) - E(T_k) \tag{9}$$

where the terms in the second member refer to L_i, R_j and T_k binding energies, respectively. The RAE edge E_{edge} is the maximum photon energy that can be emitted in a RAE process, corresponding to an Auger electron ejected with zero kinetic energy; therefore:

$$E_{edge} = E(L_i) - E(R_j) - E(T_k) \tag{10}$$

This edge is thus the difference between the energy of the diagram line $E(L_i) - E(R_j)$ and the Auger electron binding energy $E(T_k)$. The energy of the RAE band maximum E_m is always close to and below this edge. Therefore, Eq. 10 can be written as:

$$E_m \lesssim E_{edge} = E(L_iR_j) - E(T_k) \tag{11}$$

where $E(L_iR_j)$ is the energy of the L_iR_j transition. Thus, the energy shift of a RAE structure with respect to the parent line should satisfy:

$$E(L_iR_j) - E_m \gtrsim E(T_k) \tag{12}$$

Then, from Eq. 12, it is possible to associate each RAE structure found from the spectral processing with a particular absorption edge. According to this criterion, the RAEs observed for Ru, Ag and Te can be related to the $N_{4,5}$, $N_{4,5}$ and $O_{2,3}$ absorption edges, respectively. This assignment arises by considering the absorption edges given in Zschornack[20], which are in the ranges 1.8–2.4, 3.0–3.6 and 2.0–2.6 eV, while the ΔE values obtained here (see Table 6) are in the ranges 2.4–2.7, 3.1–5.1 and 4.8–7.3 eV, respectively.

5 Conclusion

The X-ray emission involving atomic decays to the L-shell vacancy states of Ru, Ag and Te was studied experimentally. To this end, spectra induced by electron impact were measured by wavelength
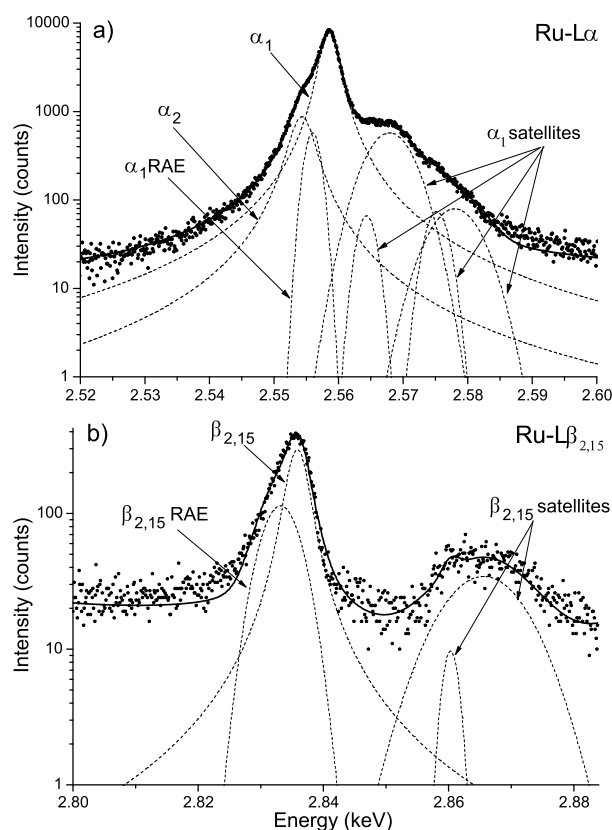
Fig. 5 X-ray spectra of Ru in the Lα (a) and L$\beta_{2,15}$ (b) regions. Dots: experimental spectrum; solid line: spectral fitting; dashed line: contribution of each diagram, satellite and RAE transition.
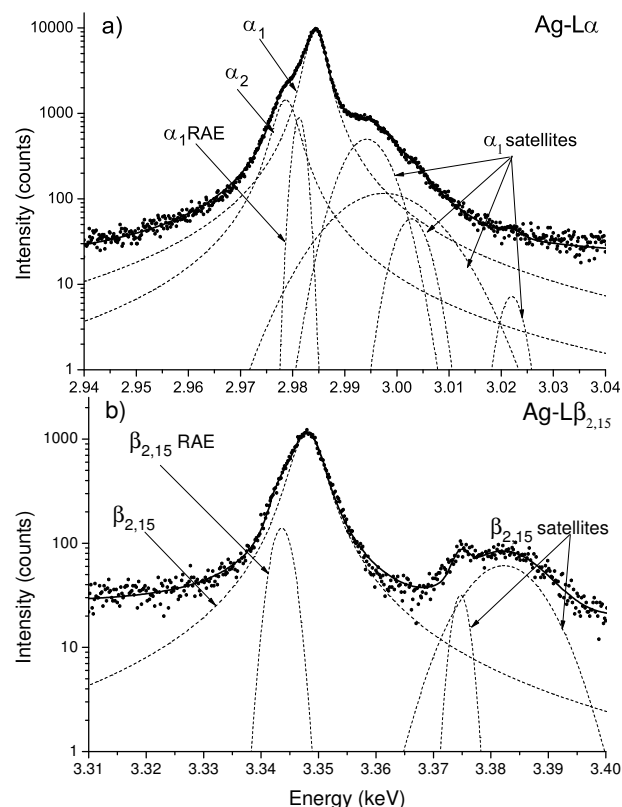

Fig. 6 X-ray spectra of Ag in the Lα (a) and L$\beta_{2,15}$ (b) regions. Dots: experimental spectrum; solid line: spectral fitting; dashed line: contribution of each diagram, satellite and RAE transition.

dispersive spectrometry and processed by a parameter optimization method. A set of 12, 14 and 17 diagram transitions were studied for Ru, Ag and Te, respectively.

Regarding the characteristic energies and natural linewidths, the values obtained in the present work are in good agreement with data given by other authors in most of the cases, except for the results published by Perkins et al.[13]. Particularly, the characteristic energies given by these authors exhibit large discrepancies with the results presented here and the experimental and theoretical data available in the literature. On the other hand, the general agreement of the present results with the calculations performed by Deslattes et al.[11] supports the framework of the relativistic many-body problem in atoms used by them. There exist discrepancies between the present data and values published by other authors for some characteristic energies corresponding to weak transitions, and for two natural linewidths ($L_3N_{4,5}$ and L_2N_4 lines) of Te. It must be pointed out, however, that the natural linewidths published both in Perkins et al.[13] and Campbell and Papp[14] (chosen for the present comparison), were calculated by using the same database for the N level widths, the agreement

between them being therefore expectable.

No data were found in the literature to compare with the linewidths reported here for the Te L_3O_1 and $L_1O_{2,3}$ transitions. Some atomic level widths not previously published were determined from natural linewidths obtained here and atomic level widths given by other authors.

A detailed study of the L satellite lines of Ru, Ag and Te was faced. The energies and relative intensities obtained were compared with the few data available. It was possible to identify most of the satellite structures found here with some of the ones previously reported, in spite of the different energy resolutions and spectral processing methods of the different studies. In addition, the relative areas presented here for Ru and Te were not reported in the previous works.

Finally, the radiative Auger emission was investigated, which led to the characterization of several spectral structures not previously studied. In each case, the energy corresponding to the maximum intensity and the area relative to the parent line were determined, and the atomic level of the Auger electron was identified. These analyses were possible due to the robustness of the spectral processing method used, which allowed a detailed
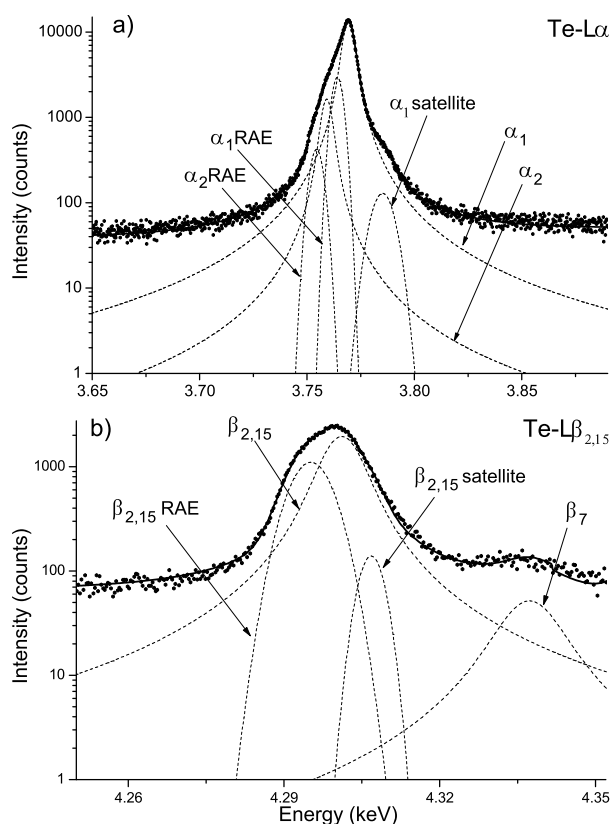
Fig. 7 X-ray spectra of Te in the Lα (a) and Lβ$_{2,15}$ (b) regions. Dots: experimental spectrum; solid line: spectral fitting; dashed line: contribution of each diagram, satellite and RAE transition.

description of complicated structures, in spectra measured with a commercial wavelength dispersive spectrometer attached to a scanning electron microscope.

Acknowledgements

References

1 M. Ertugrul, J. Anal. At. Spectrom., *2002*, **17**, *400–405*.

2 M. K. S. Fazinić, L. Mandić and I. Božičević, J. Anal. At. Spectrom., *2011*, **26**, *2467–2476*.

3 S. Limandri, A. Carreras, R. Bonetto and J. Trincavelli, Phys. Rev. A, *2010*, **81**, *012504 1–10*.

4 I. B. S. Fazinić and L. Mandić, J. Anal. At. Spectrom., *2013*, **28**, *1725–1733*.

5 R. Bonetto, G. Castellano and J. Trincavelli, X-Ray Spectrom., *2001*, **30**, *313–319*.

6 J. A. Bearden, Rev. Mod. Phys, *1967*, **39**, *78*.

7 Y. Cauchois and C. Sénémaud, Wavelengths of x-ray emission lines and absorption edges, *Pergamon Press, Oxford, 1978, vol. 18*.

8 M. Ohno, P. Putila-Mantyla and G. Graeffe, J. Phys. B, *1984*, **17**, *1747–1754*.

9 L. G. Parratt, Phys. Rev., *1938*, **54**, *99*.

10 P. Indelicato, S. Boucard and E. Lindroth, Eur.Phys. J. D, *1998*, **3**, *29–41*.

11 R. D. Deslattes, E. G. Kessler Jr., P. Indelicato, L. de Billy, E. Lindroth and J. Anton, Rev. Mod. Phys., *2003*, **75**, *35–99*.

12 J. H. Scofield, Phys. Rev. A, *1974*, **10**, *1507*.

13 S. T. Perkins, D. E. Cullen, M. H. Chen, J. H. Hubbell, J. Rathkopf and J. H. Scofield, Lawrence Livermore National Laboratory Report, *1991*, **UCRL-50400 30**, *1*.

14 J. L. Campbell and T. Papp, At. Data Nucl. Data Tables, *2001*, **77**, *1–56*.

15 S. Limandri, J. Trincavelli, R. Bonetto and A. Carreras, Phys. Rev. A, *2008*, **78**, *022518 1–10*.

16 S. J. B. Reed, Electron microprobe analysis, *Cambridge University Press, Cambridge, 2nd edn, 1997*.

17 J. Trincavelli, S. Limandri, A. Carreras and R. Bonetto, Microsc. Microanal., *2008*, **14**, *306*.

18 R. D. Bonetto, A. C. Carreras, J. C. Trincavelli and G. E. Castellano, J. Phys. B, *2004*, **37**, *1477*.

19 J. H. Scofield, At. Data Nucl. Data Tables, *1974*, **14**, *121*.

20 G. Zschornack, Handbook of X-Ray Data, *Springer-Verlag, Berlin, 2007*.